COMPDYN 2011
3rd ECCOMAS Thematic Conference on
Computational Methods in Structural Dynamics and Earthquake Engineering
M. Papadrakakis, M. Fragiadakis, V. Plevris (eds.)
Corfu, Greece, 25–28 May 2011

THE ROCKING RESPONSE OF SEISMICALLY ISOLATED, FREE-STANDING RIGID BLOCKS.

Michalis F. Vassiliou and Nicos Makris

Department of Civil Engineering University of Patras, Patras GR26500, Greece
email: mfvassiliou@gmail.com
nmakris@upatras.gr

Keywords: Rocking Columns, Seismic Isolation, Spherical Sliding Bearings, Earthquake Engineering

Abstract. This paper examines the rocking response and stability of rigid blocks standing free on an isolated base supported on linear viscoelastic bearings and bearings that exhibit bilinear behavior. The investigation concludes that seismic isolation is beneficial only for small blocks. This happens because while seismic isolation increase the "static" value of the minimum overturning acceleration, this acceleration value remains nearly constant as we move towards larger blocks or higher frequency pulses; therefore seismic isolation removes drastically from the dynamics of rocking blocks the beneficial property of increasing stability as their size increases or as the excitation pulse period decreases. This remarkable result suggests that freestanding ancient classical columns exhibit superior stability as they are built (standing free on a rigid foundation) rather than if they were seismically isolated even with isolation systems with very long isolation periods. The study further confirms this finding by examining the seismic response of the columns from the peristyle of two ancient Greek temples when subjected to historic records.

1 INTRODUCTION

Under base shaking slender objects and tall rigid structures may enter into rocking motion that occasionally results in overturning. Early studies on the rocking response of a rigid block supported on a base undergoing horizontal accelerated motion were presented by Housner (1963) [1]. His pioneering work uncovered a size-frequency scale effect which explained why: (a) the larger of two geometrically similar blocks can survive the excitation that will topple the smaller block; and (b) out of two same acceleration-amplitude pulses the one with the longer duration is more capable to induce overturning.

As the size of the block increases, the duration of the coherent pulse of the base motion plays a dominant role in inducing overturning. For instance, Figure 1, plots the rocking response of a rigid block that is 2.0m tall and 0.5m wide when subjected to an intense (a_p=0.5g) but short duration (T_p=0.5s) one-sine acceleration pulse (left–no overturning) and a less intense (a_p=0.29g), yet longer duration pulse (T_p=2s) one sine acceleration pulse (right – overturning). Interestingly, this 2.0m×0.5m rigid block survives the intense, short duration pulse; yet overturns when subjected to the lower acceleration amplitude, long-duration pulse. The above example shows that reducing the base acceleration while lengthening the period of the excitation (what seismic isolation does) is not a beneficial approach for all combinations of block size and frequency content of the base excitation.

The rocking response of slender rigid objects standing free on a seismically isolated base is a subject that has received attention during the last two decades mainly from the need to protect slender art objects within museums (Augusti et al. 1992 [2], Vestroni and Di Cinto 2000 [3], Calio and Marletta 2003 [4], Roussis et al. 2008 [5], Contento and Egidio 2009 [6]

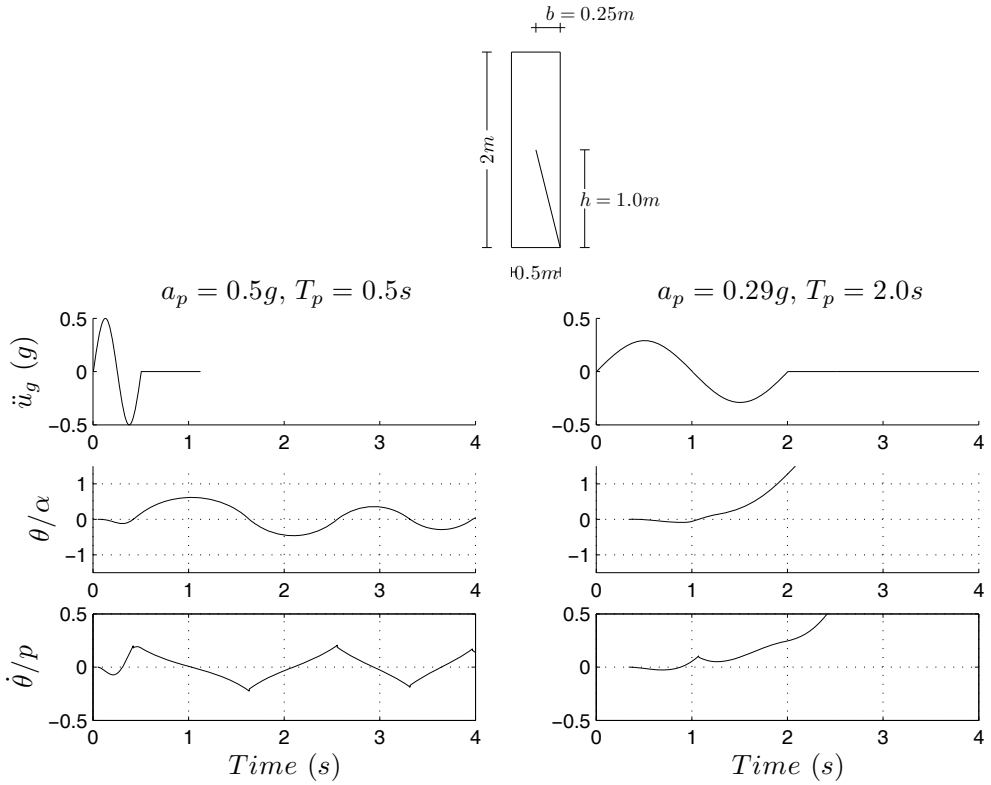

Figure 1. Horizontal ground acceleration, block rotation and angular velocity time histories of the block shown above (p=2.67rad/s, tan(α)=0.25) subjected to a one-sine pulse. Left: a_p=0.50g, T_p=0.5s – no overturning, Right a_p=0.29g<0.5g and T_p=2.0s>0.5s – overturning.

among others). These studies primarily focused on the seismic protection of relative small size blocks such as art objects up to human-size statues and they invariably concluded that seismic isolation suppresses the rocking response and protects such objects from overturning. Given, however, the results of Figure 1, this paper investigates in depth up to what size of free standing objects the application of seismic isolation is beneficial and concludes that larger free-standing structures like ancient columns of temples have superior stability as they stand free atop their massive foundations compare to if they were seismic isolated. Furthermore, this study settles the matter of conservation of linear momentum of the entire system (the rocking – translating block and the translating isolated base) during the impact of the rocking block – a matter that has been overlooked by other investigators.

2 REVIEW OF THE ROCKING RESPONSE OF A RIGID BLOCK.

With reference to Figure 2 and assuming that the coefficient of friction is large enough so that there is no sliding, the equation of motion of a rocking block with size $R=\sqrt{h^2+b^2}$ and slenderness α=atan(b/h) for rotation around O and O' respectively is (Yim et al. 1980 [7], Makris and Roussos 2000 [8], Zhang and Makris 2001 [9] among others)

$$I_o\ddot{\theta}(t)+mgR\sin\left[-\alpha-\theta(t)\right]=-m\ddot{u}_g(t)R\cos\left[-\alpha-\theta(t)\right],\quad \theta(t)<0 \tag{1}$$

$$I_o\ddot{\theta}(t)+mgR\sin\left[\alpha-\theta(t)\right]=-m\ddot{u}_g(t)R\cos\left[\alpha-\theta(t)\right],\quad \theta(t)>0. \tag{2}$$

For rectangular blocks, $I_o=(4/3)mR^2$ and the above equations can be expressed in the compact form

$$\ddot{\theta}(t)=-p^2\left\{\sin\left[\alpha\,\mathrm{sgn}\left(\theta(t)\right)-\theta(t)\right]+\frac{\ddot{u}_g}{g}\cos\left[\alpha\,\mathrm{sgn}\left(\theta(t)\right)-\theta(t)\right]\right\}. \tag{3}$$

The oscillation frequency of a rigid block under free vibration is not constant, because it strongly depends on the vibration amplitude (Housner 1963 [1]). Nevertheless, the quantity

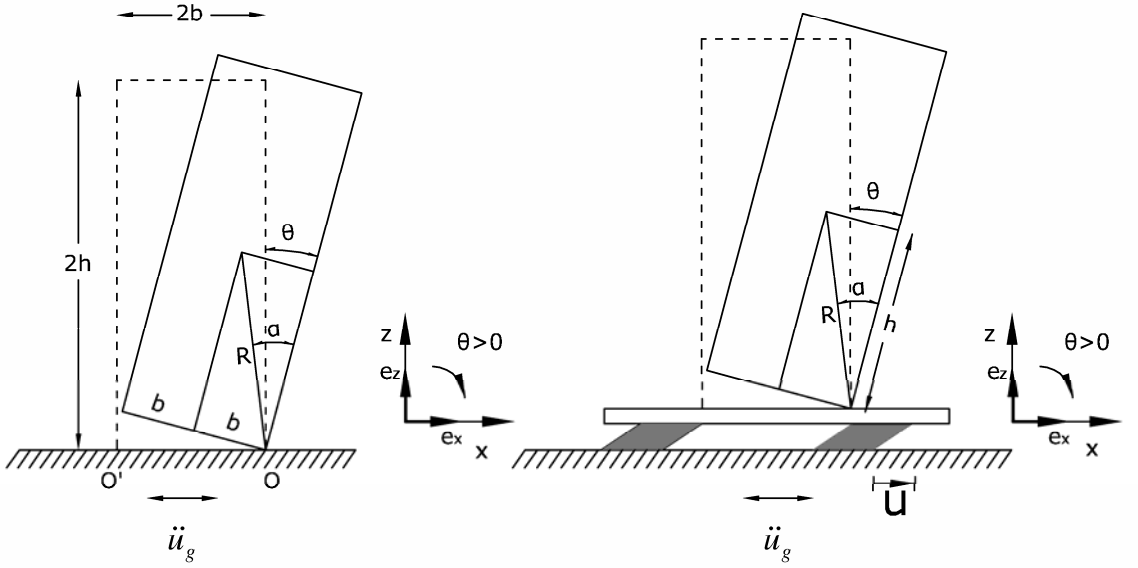

Figure 2. Geometric characteristics of the model considered. Left: Rigid block subjected to ground shaking. Right: Rigid block on isolated base.

$p = \sqrt{\frac{3g}{4R}}$ is a measure of the dynamic characteristics of the block. For the 2.0m×0.5m block shown in Figure 1 (say an modern refrigerator), $p = 2.67$ *rad/s*, and for a household brick, $p \approx 8$ *rad/s*.

Figure 3 shows the moment-rotation relationship during the rocking motion of a free-standing block. The system has infinite stiffness until the magnitude of the applied moment reaches the value $mgR\sin\alpha$, and once the block is rocking, its restoring force decreases monotonically, reaching zero when $\theta = \alpha$. During the oscillatory rocking motion, the moment-rotation curve follows this curve without enclosing any area. Energy is lost only during impact, when the angle of rotation reverses. When the angle of rotation reverses, it is assumed that the rotation continues smoothly from points O to O' and that the impact force is concentrated at the new pivot point, O'. With this idealization, the impact force applies no moment around O', hence the angular momentum around O' is conserved. Conservation of angular momentum about point O' just before the impact and right after the impact gives

$$I_o\dot{\theta}_1 - m\dot{\theta}_1 2bR\sin(\alpha) = I_o\dot{\theta}_2 \tag{4}$$

where $\dot{\theta}_1$ = angular velocity just prior to the impact; and $\dot{\theta}_2$ = angular velocity right after the impact. The ratio of kinetic energy after and before the impact is

$$r = \frac{\dot{\theta}_2^2}{\dot{\theta}_1^2} \tag{5}$$

which means that the angular velocity after the impact is only $\sqrt{r}$ times the velocity before the impact. Substitution of (4) into (5) gives

$$r = [1 - \frac{3}{2}\sin^2\alpha]^2 \tag{6}$$

The value of the coefficient of restitution given by (6) is the maximum value of r under which a block with slenderness α will undergo rocking motion. Consequently, to observe rocking motion, the impact has to be inelastic. The less slender a block (larger α), the more plastic is the impact, and for the value of $\alpha = \sin^{-1}\sqrt{2/3} = 54.73^o$, the impact is perfectly plastic.

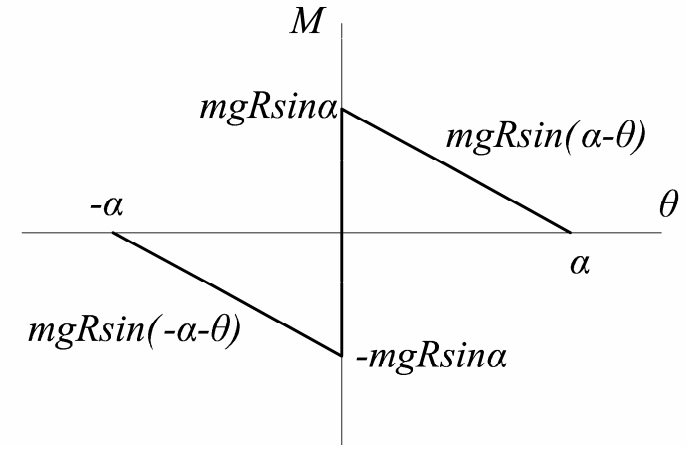

Figure 3. Moment rotation diagram of a rocking object

During rocking motion of slender blocks, if additional energy is lost due to the inelastic behavior at the instant of impact, the value of the true coefficient of restitution r will be less than the one computed from equation (6).

3 TIME SCALE AND LENGTH SCALE OF PULSE-LIKE GROUND MOTIONS

The relative simple form, yet destructive potential of near source ground motions has motivated the development of various closed form expressions which approximate their leading kinematic characteristics. The early work of Veletsos et al. [10] was followed by the papers of Hall et al. [11], Heaton et al. [12], Makris [13], Makris and Chang [14], Alavi and Krawinkler [15] and more recently by the paper of Mavroeidis and Papageorgiou [16]. Some of the proposed pulses are physically realizable motions with zero final ground velocity and finite accelerations whereas some other idealizations violate one or both of the above requirements. Physically realizable pulses can adequately describe the impulsive character of near-fault ground motions both qualitatively and quantitatively. The input parameters of the model have an unambiguous physical meaning. The minimum number of parameters is two, which are either the acceleration amplitude, a_p, and duration, T_p, or the velocity amplitude, v_p, and duration, T_p (Makris 1997[13], Makris and Chang 2000[14]). The more sophisticated model of Mavroeidis and Papageorgiou [16] involves 4 parameters, which are the pulse period, the pulse amplitude as well as the phase and number of half cycles, and was found to describe a large set of velocity pulses generated due to forward directivity or permanent translation effect. The pulse period, T_p, of the most energetic pulse of strong ground motions is strongly correlated with the moment magnitude, M_w, of the event. For a given moment magnitude, the duration of pulses produced by strike-slip faults is on average larger than the duration of pulses generated by reverse faults. Assuming that the time scale T_p is independent of the source–station distance, for stations located within ~10km from the causative fault, the pulse period and moment magnitude are related through the following empirical relationship which also satisfies a self-similarity condition [16, 17, 18]:

$$\ln T_p = -2.9 + 0.5 M_w \tag{7}$$

Furthermore, seismological data indicate that the amplitude of the velocity pulses recorded within a distance of 7 km from the causative fault varies from 60 to 120 cm/s. This observation is in good agreement with the typical slip velocity value of 90 cm/s frequently considered by seismologists (Brune 1970 [19], Aki 1983[20]).

The current established methodologies for estimating the pulse characteristics of a wide class of records are of unique value since the product, $a_p T_p^2 = L_p$, is a characteristic length scale of the ground excitation and is a measure of the persistence of the most energetic pulse to generate inelastic deformations (Makris and Black 2004 [21]). It is emphasized that the persistence of the pulse is a different characteristic than the strength of the pulse which is measured with the peak pulse acceleration. The reader should recall that among two pulses with different acceleration amplitude (say $a_{p1} > a_{p2}$) and different pulse duration (say $T_{p1} < T_{p2}$), the inelastic deformation does not scale with the peak pulse acceleration (most intense pulse) but with the stronger length scale (larger $a_p T_p^2$ = most persistent pulse), Makris and Black 2004a,b [21],[22], Karavassilis et al. 2010 [23].

The heavy line in Figure 4 (top) which approximates the long-period acceleration pulse of the NS component of the 1992 Erzinkan, Turkey, record is a scaled expression of the second derivative of the Gaussian distribution, $e^{-\frac{t^2}{2}}$, known in the seismology literature as the

symmetric Ricker wavelet (Ricker 1943[24], 1944[25]) and widely referred as the "Mexican Hat" wavelet, Addison 2002[26])

$$\ddot{u}_g(t) = a_p\left(1 - \frac{2\pi^2 t^2}{T_p^2}\right)e^{-\frac{1}{2}\frac{2\pi^2 t^2}{T_p^2}} \tag{8}$$

The value of $T_p = \frac{2\pi}{\omega_p}$, is the period that maximizes the Fourier spectrum of the symmetric Ricker wavelet.

Similarly, the heavy line in Figure 4 (center) which approximates the long-period acceleration pulse of the Pacoima Dam motion recorded during the February 9, 1971 San Fernando, California earthquake is a scaled expression of the third derivative of the Gaussian

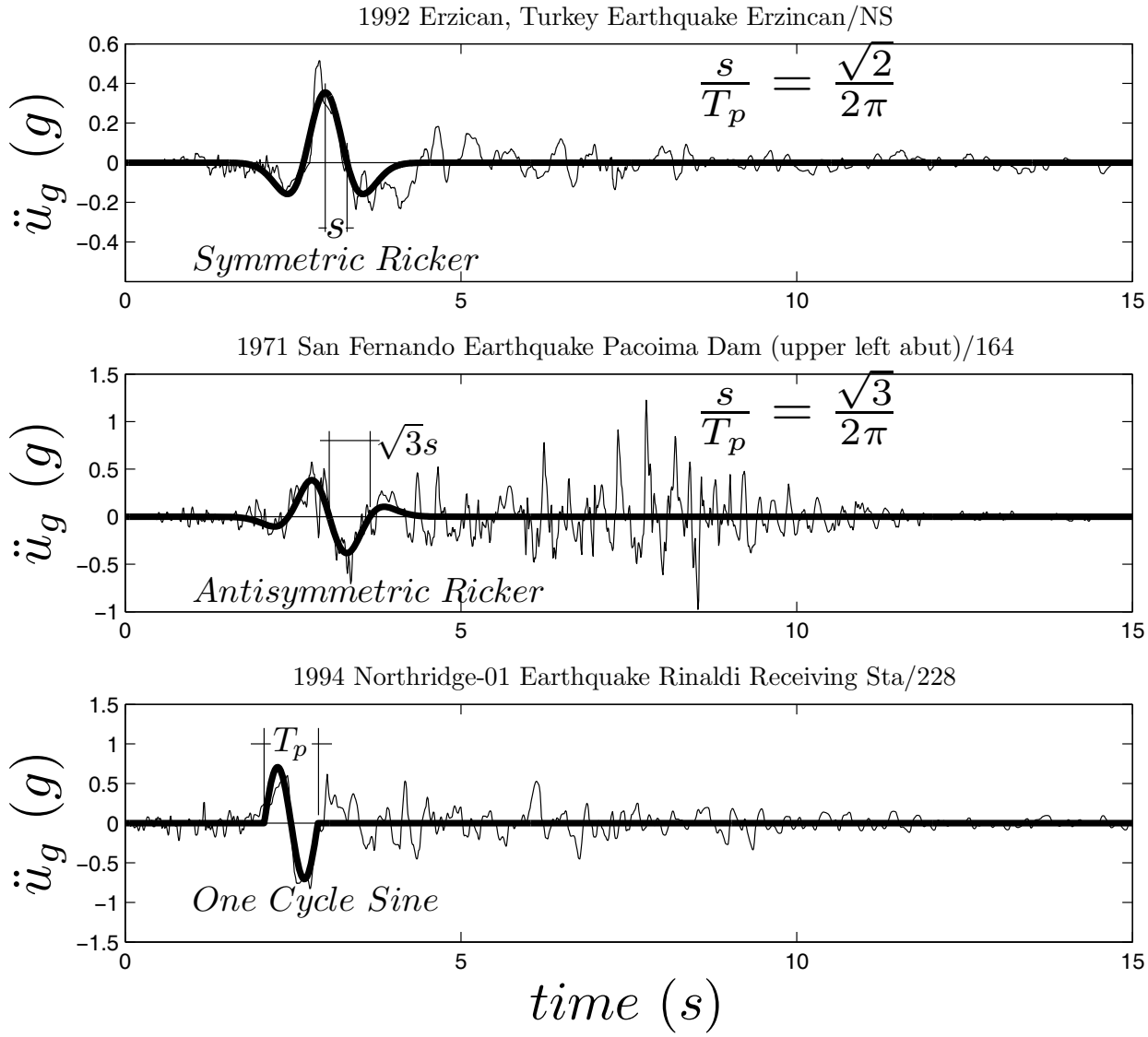

Figure 4. Acceleration time histories recorded during the: (Top) 1992 Erzincan, Turkey earthquake together with a symmetric Ricker wavelet; (Center) 1971 San Fernando earthquake – fault normalcomponent of the Pacoima Dam record together with an antisymmetric Ricker wavelet; and (bottom) 1994 Northridge earthquake – 228 Rinaldi station together with a one cycle sine pulse.

distribution $e^{-\frac{t^2}{2}}$. Again, in equation (18) the value of $T_p = \frac{2\pi}{\omega_p}$ is the period that maximizes the Fourier spectrum of the antisymmetric Ricker wavelet.

$$\ddot{u}_g(t) = \frac{a_p}{\beta}\left(\frac{4\pi^2 t^2}{3T_p^2} - 3\right)\frac{2\pi t}{\sqrt{3}T_p} e^{-\frac{1}{2}\frac{4\pi^2 t^2}{3T_p^2}} \tag{9}$$

in which β is a factor equal to 1.38 that enforces the above function to have a maximum – a_p.

The choice of the specific functional expression to approximate the main pulse of pulse–type ground motions has limited significance in this work. In the past simple trigonometric pulses have been used by the senior author (Makris 1997[13], Makris and Chang 2000[14], Makris and Black 2004[21],[22]) to extract the time scale and length scale of pulse-type ground motions. For instance the heavy line in Figure 4 (bottom) which approximates the strong coherent acceleration pulse of the 228 component at the Rinaldi receiving station of the 1994 Northridge earthquake is a one-sine acceleration pulse

$$\ddot{u}_g(t) = a_p \sin(\omega_p t), \qquad 0 < t < T_p \tag{10}$$

A mathematically rigorous and easily reproducible methodology based on wavelet analysis to construct the best matching wavelet on a given record (signal) has been recently proposed by Vassiliou and Makris (2009)[27,28].

5 OVERTURNING SPECTRA – SELF-SIMILAR RESPONSE

Consider a free standing rigid block subjected to an acceleration pulse (like those shown in Figure 4) with acceleration amplitude a_p and pulse duration $T_p = \frac{2\pi}{\omega_p}$. From equation (3) it results that the response of a rocking block subjected to an acceleration pulse is a function of five variables

$$\theta(t) = f\left(p, \alpha, g, a_p, \omega_p\right) \tag{11}$$

The six (6) variables appearing in Equation (11), $\theta \doteq [\ ]$, $a_p \doteq [\mathrm{L}][\mathrm{T}]^{-2}$, $\omega_p \doteq [\mathrm{T}]^{-1}$, $p \doteq [\mathrm{T}]^{-1}$, $\alpha \doteq [\ ]$, $g \doteq [\mathrm{L}][\mathrm{T}]^{-2}$ involve only two reference dimensions; that of length [L] and time [T]. According to Buckingham's Π-theorem the number of dimensionless products with which the problem can be completely described is equal to [number of variables in Eq. (11)= 6] – [number of reference dimensions = 2]. Herein we select as repeating variables the characteristics of the pulse excitation, a_p and ω_p. The four independent Π-terms are

$$\Pi_\theta = \theta \tag{12}$$

$$\Pi_\omega = \frac{\omega_p}{p} \tag{13}$$

$$\Pi_\alpha = \tan(\alpha) \tag{14}$$

$$\Pi_g = \frac{a_p}{g} \tag{15}$$

With the four dimensionless Π-Terms established equation (11) reduces to

$$\theta(t) = \varphi(\frac{\omega_p}{p}, \tan\alpha, \frac{\alpha_p}{g}) \tag{16}$$

The rocking response of a rigid block when subjected to a horizontal base acceleration, $\ddot{u}_g(t)$, is computed by solving equation (3) in association with the minimum energy loss expressions given by equation (6) which takes place at every impact. The solution of the nonlinear differential equation given by (3) is computed numerically by means of a state-space formulation. The state vector of the system shown in Figure 2 (left) is merely

$$\mathbf{y(t)} = \begin{bmatrix} \theta(t) \\ \dot{\theta}(t) \end{bmatrix} \tag{17}$$

and the time-derivative vector $\mathbf{f(t) = \dot{y}(t)}$ is

$$\dot{\mathbf{y}}\mathbf{(t)} = \begin{bmatrix} \dot{\theta}(t) \\ -p^2[\sin[\alpha\,\mathrm{sgn}[\theta(t)] - \theta(t)] + \frac{\ddot{u}_g(t)}{g}\cos[\alpha\,\mathrm{sgn}[\theta(t)] - \theta(t)] \end{bmatrix} \tag{18}$$

The numerical integration of (18) is performed with standard Ordinary Differential Equations (ODE) solvers available in MATLAB (The Mathworks, 1992) [29].

Figure 5 shows the overturning acceleration spectrum of a rigid block with slenderness α = 14° due to a one sine acceleration pulse (left) , a symmetric Ricker wavelet (center) and an antisymmetric Ricker wavelet (right). Figure 5 indicates that as $\Pi_\omega = \frac{\omega_p}{p}$ increases the acceleration needed to overturn the object becomes appreciably larger than the one needed to uplift it.

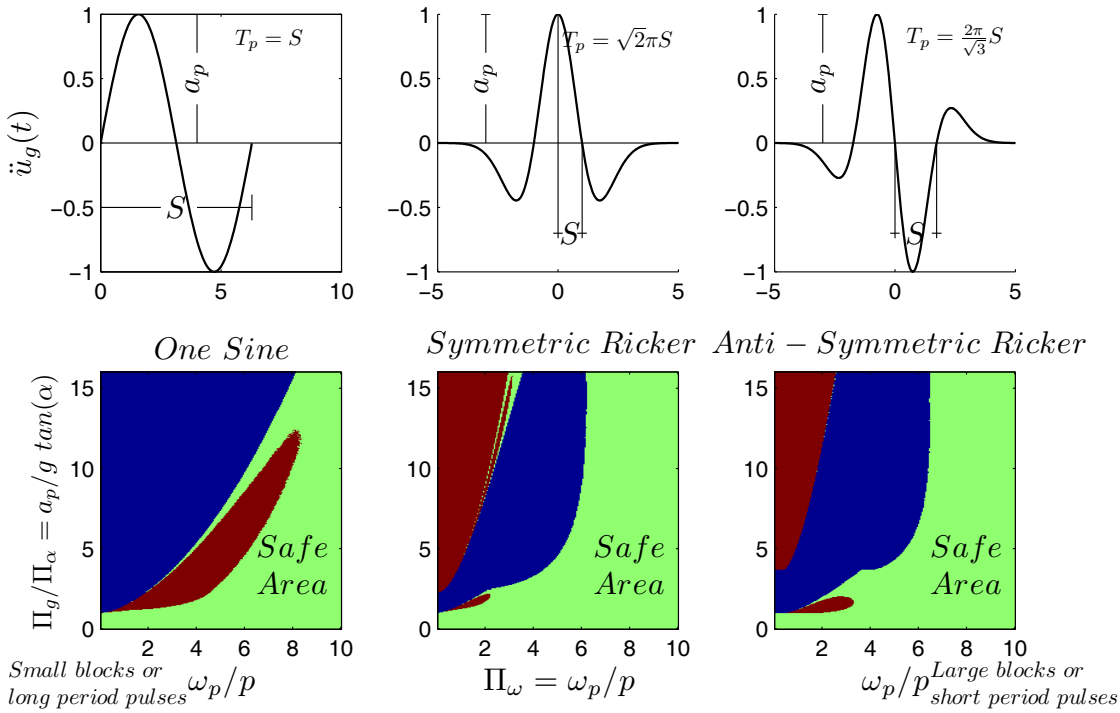

Figure 5 Overturning acceleration spectra of a free standing block with slenderness α=14° subjected to a one-sine acceleration pulse (left); a symmetric Ricker wavelet (center) and an antisymmetric Ricker wavelet (right)

The light grey (green in the colored version) area in all three bottom plots corresponds to stability (no overturning). Note that all three plots show that there are safe areas above the minimum overturning acceleration – a behavior that results from the strong nonlinear nature of the problem. Most importantly is that as the ratio $\Pi_\omega=\omega_p/p$ increases (shorter duration pulses or larger blocks) the minimum overturning acceleration needed to overturn the block increases appreciably.

6 ROCKING RESPONSE OF A RIGID BLOCK STANDING FREE ON A SEISMICALLY ISOLATED BASE

6.1 Linear Viscoelastic Isolation System

We consider a rigid block with mass, m, slenderness α, and frequency parameter p, standing free on a seismically isolated base with mass m_b, horizontal linear stiffness k_b and viscous damping c_b, as shown in Figure 2 (right). The equation of motion can be derived from equation (3) by substituting $\ddot{u}_g$ with $\ddot{u}_g+\ddot{u}$ where u is the displacement of the isolated base relative to the ground. Then equation (3) becomes

$$\ddot{\theta}(t)=-p^2\left\{\sin\left[\alpha\,\mathrm{sgn}\left(\theta(t)\right)-\theta(t)\right]+\frac{\ddot{u}_g(t)+\ddot{u}(t)}{g}\cos\left[\alpha\,\mathrm{sgn}\left(\theta(t)\right)-\theta(t)\right]\right\} \tag{19}$$

Moreover, given that there is no sliding, horizontal force equilibrium of the isolated base below isolators gives

$$-k_b u-c_b\dot{u}=m_b\left(\ddot{u}_g+\ddot{u}\right)+m\left(\ddot{u}_g+\ddot{u}+\ddot{x}\right) \tag{20}$$

where x is the horizontal, relative to the base translation of the center of mass of the rigid block given by

$$x(t)=\mathrm{sgn}\left(\theta(t)\right)R\sin(a)-R\sin\left(\mathrm{sgn}\left(\theta(t)\right)\alpha-\theta(t)\right) \tag{21}$$

Equations (19) and (20) are expressed in terms of $\ddot{u}$ and $\ddot{\theta}$ which are explicit expressions of the four states of the system, $u(t),\dot{u}(t),\theta(t),\dot{\theta}(t)$ in order to solve the system of equations explicitly. Accordingly,

$$\ddot{u}(t)=\frac{-\omega_b^2u(t)-2\xi\omega_n\dot{u}(t)-\gamma R\left(\dot{\theta}(t)\right)^2\sin A(t)+\gamma Rp^2\cos A(t)\sin A(t)}{1-\dfrac{\gamma Rp^2\cos^2 A(t)}{g}}-\ddot{u}_g(t) \tag{22}$$

$$\ddot{\theta}(t)=-p^2\left(\sin A(t)+\cos A(t)\left(\frac{-\omega_n^2u(t)-2\xi\omega_n\dot{u}(t)-\gamma R\left(\dot{\theta}(t)\right)^2\sin A(t)+\gamma Rp^2\cos A(t)\sin A(t)}{g-\gamma Rp^2\cos^2 A(t)}\right)\right) \tag{23}$$

where the term $A(t)=\alpha\,\mathrm{sgn}\,\theta(t)-\theta(t)$ and $\gamma=\dfrac{m}{m_b+m}$ and $\omega_b=\sqrt{\dfrac{k_b}{m_b+m}}$

Again, in this case we assume that when the angle of rotation reverses, the rotation of the block continues smoothly from point O to O' and that the impact force is concentrated as a point force which applies on the new pivot point O'. The subtle difference between a rocking

block impacting a base with finite mass, m_b, and a rocking block impacting a rigid foundation with infinite mass, is that the translational velocity of the isolated base also experiences a finite jump during impact; whereas the translational velocity of the rigid foundation with infinite mass remains the same during impact.

With reference to Figure 6, conservation of angular momentum around point O' gives

$$\int_{block} \mathbf{r}\times\left(\dot{\mathbf{v}}_1+\dot{\mathbf{u}}_1\right)dm = \int_{block} \mathbf{r}\times\left(\dot{\mathbf{v}}_2+\dot{\mathbf{u}}_2\right)dm \tag{24}$$

where $\dot{\mathbf{v}}_1$ and $\dot{\mathbf{v}}_2$ are the velocities (with respect to the isolated base) of a point mass due to rotation before and after the impact and $\dot{\mathbf{u}}_1$ and $\dot{\mathbf{u}}_2$ are the translational velocities of the base (with respect to the ground) before and after the impact. Equation (24) gives

$$\left(I_o\dot{\theta}_1 - 2mRb\sin\alpha\dot{\theta}_1\right)\mathbf{e}_y + \int_{block}\mathbf{r}\times\dot{\mathbf{u}}_1 dm = I_o\dot{\theta}_2\mathbf{e}_y + \int_{block}\mathbf{r}\times\dot{\mathbf{u}}_2 dm \tag{25}$$

or

$$I_o\dot{\theta}_1 - 2mRb\sin\alpha\dot{\theta}_1 + mhu_1 = I_o\dot{\theta}_2 + mhu_2\,. \tag{26}$$

For a rectangular block $I_o = \frac{4}{3}mR^2$ and the above expression reduces to

$$4R^2\dot{\theta}_1 - 6Rb\sin\alpha\dot{\theta}_1 + 3h\dot{u}_1 = 4R^2\dot{\theta}_2 + 3h\dot{u}_2 \tag{27}$$

Equation (27) indicates that because of the finite mass of the isolation base one has to determine the translational velocity of the base $\dot{u}_2$ after the impact. The extra equation that is needed to relate $\dot{u}_1$ and $\dot{u}_2$ is the conservation of the linear momentum of the entire system(the rocking – translating block together with the translating base) along the horizontal direction. Accordingly

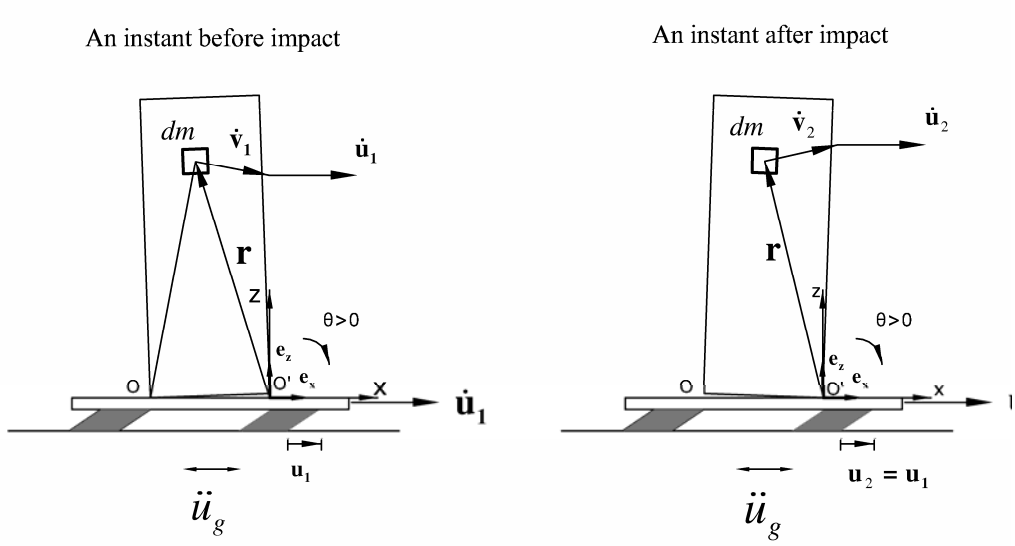

Figure 6. Rigid block rocking on an isolated base before (left) and after (right) the impact.

$$\left(m+m_b\right)\dot{u}_1+mh\dot{\theta}_1=\left(m+m_b\right)\dot{u}_2+mh\dot{\theta}_2 \tag{28}$$

or

$$\left(\gamma+1\right)\dot{u}_1+\gamma h\dot{\theta}_1=\left(\gamma+1\right)\dot{u}_2+\gamma h\dot{\theta}_2 \tag{29}$$

From equations (27) and (29) one obtains

$$\dot{\theta}_2=\frac{\left(\gamma+4\right)\cot^2\alpha-2\left(\gamma+1\right)}{\left(\gamma+4\right)\cot^2\alpha+4\left(\gamma+1\right)}\dot{\theta}_1 \tag{30}$$

and

$$\dot{u}_2=\dot{u}_1+\frac{6\gamma h}{\left(\gamma+4\right)\cot^2\alpha+4\left(\gamma+1\right)}\dot{\theta}_1 \tag{31}$$

Note that in the limiting case of a very havy base ($m_b\to\infty$ or $\gamma\to 0$) equation (30) reduces to equation (6); while $\dot{u}_1=\dot{u}_2$; therefore the situation of a block rocking on a rigid foundation is recovered. From equation (30) the maximum value of the coefficient of restitution that allows rocking motion of a block rocking on an isolated base is

$$r=\left(\frac{\dot{\theta}_2}{\dot{\theta}_1}\right)^2=\left(\frac{\left(\gamma+4\right)\cot^2\alpha-2\left(\gamma+1\right)}{\left(\gamma+4\right)\cot^2\alpha+4\left(\gamma+1\right)}\right)^2. \tag{32}$$

The expression of the coefficient of restitution given by (32) is in agreement with an equivalent expression presented by Roussis et al. [5], which, to our knowledge is the only past publication that treats this problem correctly.

Figure 7 plots the expression given by equation (32) for three values of $\gamma=m/m_b$=0.01, 0.1 and 1. Figure 7 indicates that when the mass of the base is finite, the rocking block looses additional energy during impact (compared to the same block rocking on a rigid foundation) due to the reason that the translational velocity of the isolated base experiences a finite jump at the instant of the impact.

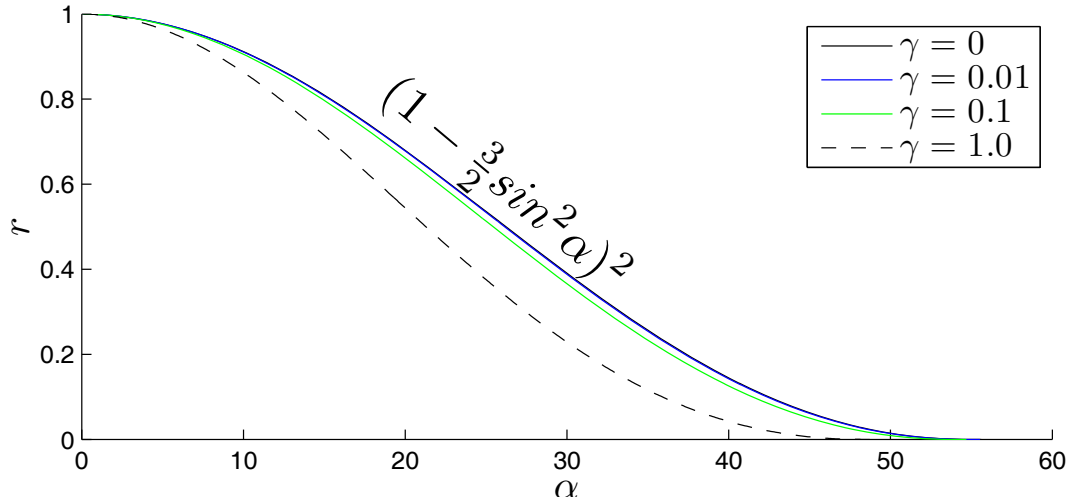

Figure 7. Coefficient of restitution, r, vs slenderness, α, for different values of $\gamma=m/m_b$.

6.2 Overturning Spectra – Self-Similar Response

We consider again that the ground excitation of the system shown in Figure 2 is characterized by a coherent acceleration pulse with amplitude a_p and pulse duration ($T_p = \frac{2\pi}{\omega_p}$). From equations (22) and (23) it results that the response of a rocking block standing free on an isolated base subjected to an acceleration pulse is a function of eight (8) variables

$$u(t) = f\left(p, \alpha, g, \omega_b, \xi, \gamma, \alpha_p, \omega_p\right) \tag{33}$$

$$\theta(t) = f\left(p, \alpha, g, \omega_b, \xi, \gamma, \alpha_p, \omega_p\right) \tag{34}$$

Each of the coupled Equations (20) and (21) $\theta \doteq [\ ]$, $u \doteq [L]$, $a_p \doteq [L][T]^{-2}$, $T_p \doteq [T]$, $T_b \doteq [T]$, $\zeta \doteq [\ ]$, $p \doteq [T]^{-1}$, $\alpha \doteq [\ ]$, $g \doteq [L][T]^{-2}$, $\gamma \doteq [\ ]$ involves only two reference dimensions; that of length [L] and time [T]. According to Buckingham's Π-theorem the number of dimensionless products (Π-Terms) = [number of variables in Eq. (20) and (21) = 10] – [number of reference dimensions = 2]; therefore for the 2 DOF system described above, there are 10-2 = 8 Π–terms

$$\Pi_m = \frac{u_{\max}\omega_p^2}{a_p} \tag{35}$$

$$\Pi_\theta = \theta \tag{36}$$

$$\Pi_\omega = \frac{\omega_b}{\omega_p} \tag{37}$$

$$\Pi_\xi = \xi \tag{38}$$

$$\Pi_\gamma = \gamma \tag{39}$$

$$\Pi_p = \frac{\omega_p}{p} \tag{40}$$

$$\Pi_a = \tan(\alpha) \tag{41}$$

$$\Pi_g = \frac{a_p}{g} \tag{42}$$

The rocking response of a rigid block standing free on an isolated base subjected to a horizontal base acceleration is computed by solving equations (21) and (22) in association with the minimum energy loss expression given by equation (32) which takes place at every impact. In this case, the state vector of the system shown in Figure 2 (right) for linear viscoelastic bearings is

$$\mathbf{y}(t) = \begin{bmatrix} u(t) \\ \dot{u}(t) \\ \theta(t) \\ \dot{\theta}(t) \end{bmatrix} \tag{43}$$

and the time derivative vector $\mathbf{f}(t) = \dot{\mathbf{y}}(t)$ is

$$\dot{\mathbf{y}}(t)=\begin{bmatrix} \dot{u}(t) \\ \dfrac{-\omega_b^2 u(t)-2\xi\omega b\dot{u}(t)-\gamma R\left(\dot{\theta}(t)\right)^2\sin A(t)+\gamma R\cos A(t)\,p^2\sin A(t)}{1-\dfrac{\gamma R p^2\cos^2 A(t)}{g}}-\ddot{u}_g(t) \\ \ddot{\theta}(t) \\ -p^2\left(\sin A(t)+\cos A(t)\left(\dfrac{-\omega_b^2 u(t)-2\xi\omega b\dot{u}(t)-\gamma R\left(\dot{\theta}(t)\right)^2\sin A(t)+\gamma R\cos A(t)\,p^2\sin A(t)}{g-\gamma R p^2\cos A(t)}\right)\right) \end{bmatrix} \tag{44}$$

Figure 8 plots the overturning acceleration spectra for a rigid block with slenderness α=10^o (top) and α=20^o (bottom) when it is standing free on a rigid foundation (left), and when it is isolated (center and right) and subjected to a symmetric Ricker wavelet. The viscous damping ratio of the bearings is ξ=5% and the mass ratio is γ=0.01 (heavy base). Figure 8 indicates that the presence of the isolation base increases the "static" overturning acceleration; however, for isolated rigid blocks this "static" value remains nearly constant as the ratio ω_p / p increases (moving to larger blocks or high frequency pulses). Consequently, the presence of an isolation base removes appreciably from the dynamics of rocking blocks the fundamental property of increasing stability as their size increases or as the excitation pulse-period decreases.

The findings of Figure 8 together with results due to an antisymmetric Ricker excitation are summarized in Figure 9 in terms of minimum acceleration overturning spectra. In all configurations the free-standing block on a rigid base (heavy dark line) beyond a certain value of ω_p/p exhibits superior stability than the same block when isolated. Note also that for both symmetric (left plots) and antisymmetric (right plots) Ricker wavelets, the minimum overturning acceleration of the free standing block on a rigid foundation exceeds the overturning acceleration of the isolated configuration at smaller values of ω_p/p as the slenderness of the block decreases (larger values of α).

The practical use of the results shown in Figure 9 is illustrated by considering the dominant pulses that capture the coherent component of the two earthquake records shown in Figure 10 – that of the fault parallel component of the OTE record from the 1995 Aigio, Greece earthquake (top) and that of the Gilroy – Array #6 record from the 1979 Coyote Lake , USA earthquake (bottom). For the FP OTE record shown in Figure 10 (top), T_p=0.6s while for the Coyote Lake record (bottom), T_p=0.9s. The corresponding values of the semidiagonal, R, beyond which non-isolated free standing blocks exhibit more stability than when seismic isolated are offered in Table 1 for two values of slenderness α=10^o and α=20^o and three values of T_b/T_p 2, 3 and 4.

Table 1 indicates that free-standing objects appreciably smaller than ancient classical columns R≈(3.5m – 5.0m) are more stable when they stand free on a rigid foundation while seismic isolation would have been detrimental.

The influence of the mass ratio $\gamma=\dfrac{m}{m+m_b}$ (m = mass of the rocking block, m_b = mass of the isolated base) is shown in Figure 11 for a block with slenderness α=12^o, two values of T_b/T_p=2 and 3 and five values of γ. Figure 11 indicates that for values of ω_p/p<6 (the range when it makes sense to isolate rocking blocks) all response curves for $\gamma\leq$0.1 tend to the finite

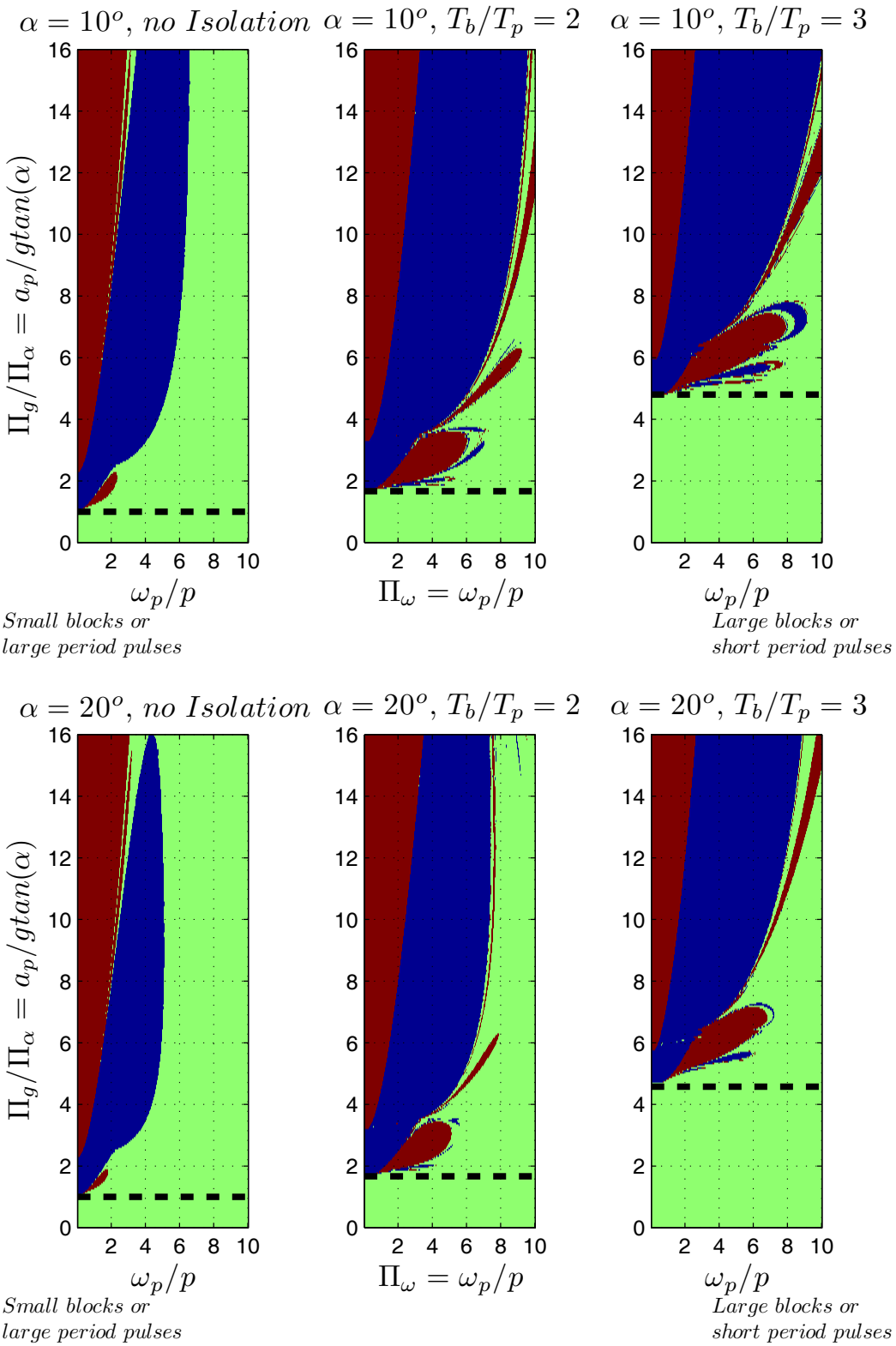

Figure 8. Overturning spectra for rigid block without isolation (left), and with linear isolation with T_b/T_p=2 (center) and T_b/T_p=3 for slenderness α=10° (top) and α=20° (bottom) for a symmetric Ricker excitation.

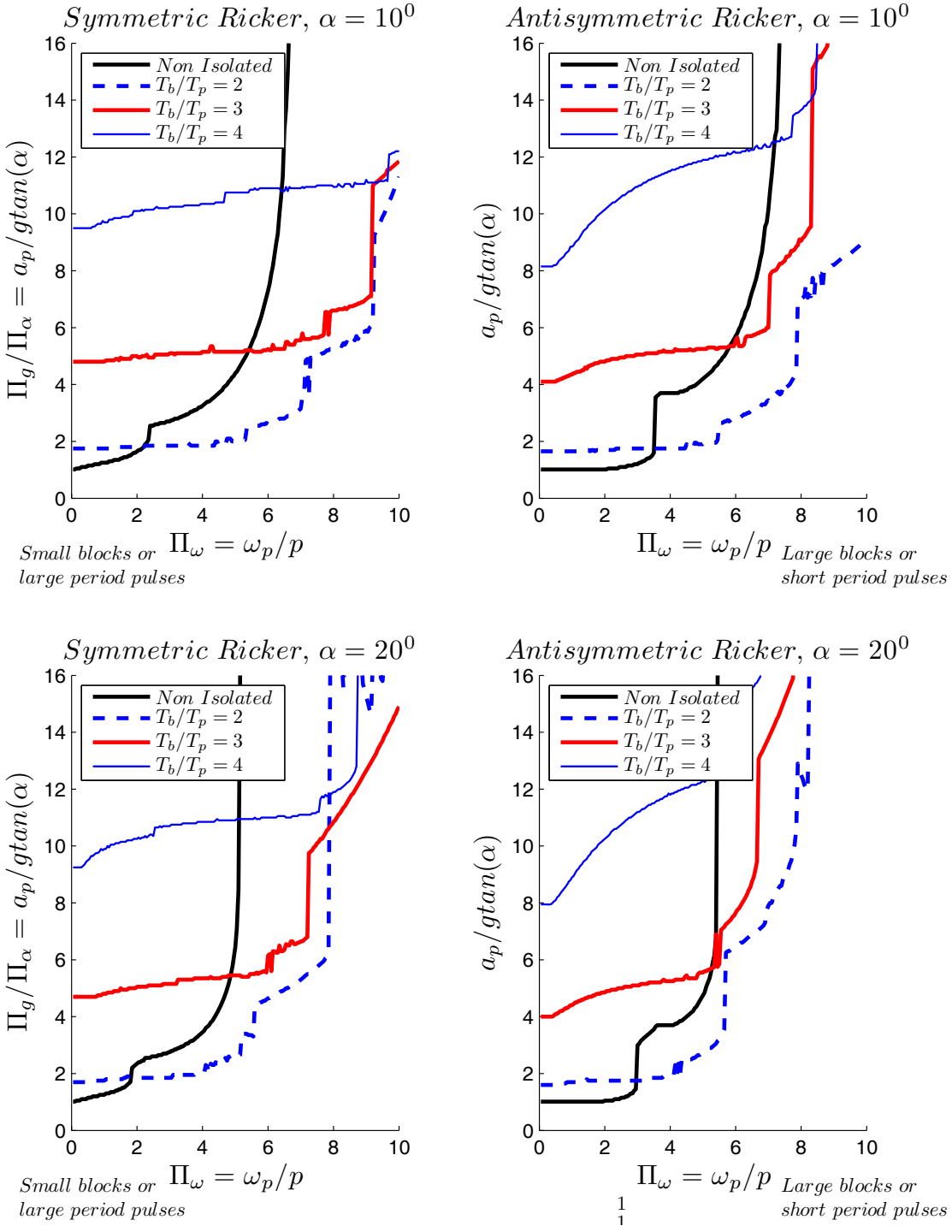

Figure 10. Comparison of the minimum acceleration needed to overturn a rigid block of slenderness α=10^o (top) and α=20^o (bottom) resting on rigid ground and on an isolated bases whith various isolation frequencies when excited by a symmetric Ricker pulse (left) or an antisymmetric Ricker pulse (right).

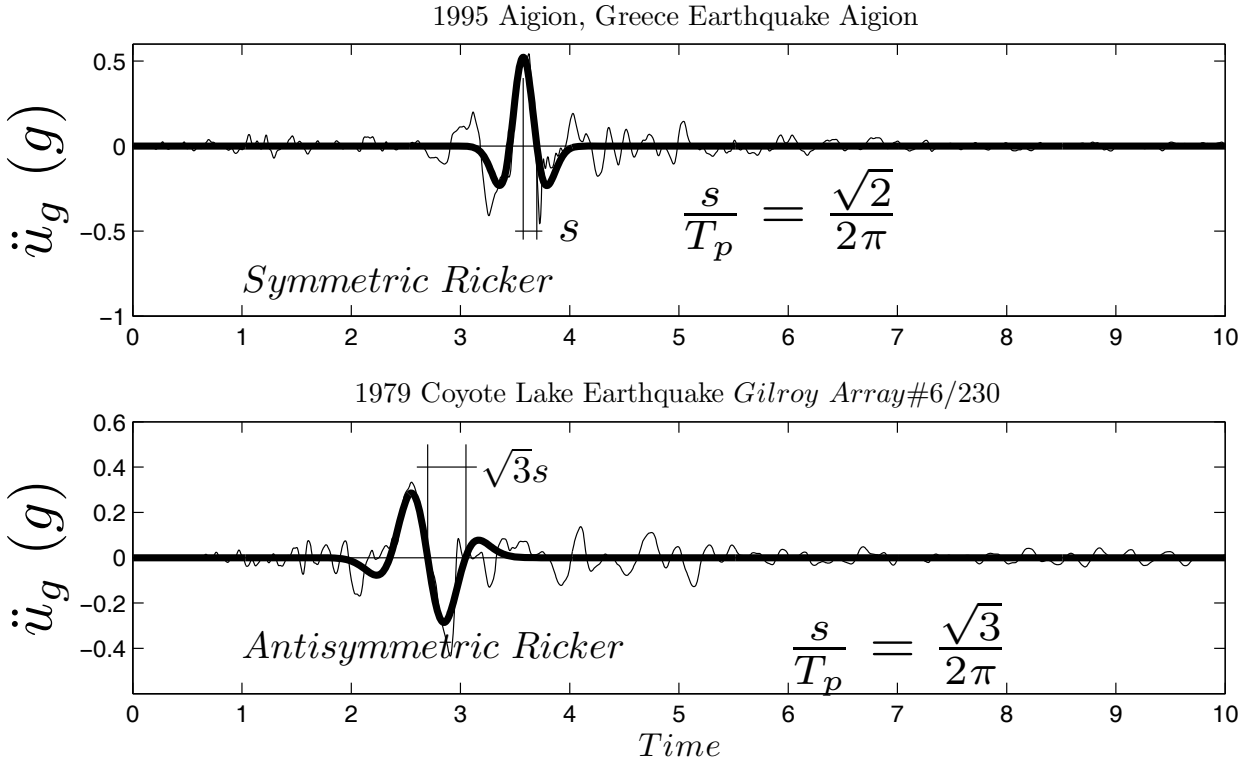

Figure 11 Acceleration time histories during the (Top) 1995 Aigion, Greece earthquake – fault parallel component of the OTE record together with a symmetric Ricker wavelet; and (bottom) 1979 Coyote Lake earthquake – 230 component of the Gilroy Array #6 record together with an antisymmetric Ricker wavelet.

		T_b/T_p=2			T_b/T_p=3			T_b/T_p=4		
			$R_{critical}$ (m)			$R_{critical}$ (m)			$R_{critical}$ (m)	
	T_p (s)	T_b (s)	10°	20°	T_b (s)	10°	20°	T_b (s)	10°	20°
Aigio, OTE FP, 1995	0.6	1.2	0.32	0.22	1.8	1.96	1.58	2.4	2.79	1.78
Coyote Lake, Gilroy #6 230, 1979	0.9	1.8	1.85	1.31	2.7	5.08	4.24	3.6	7.83	4.48

Table 1. Length of the semidiagonal, R, of rigid blocks beyond which they exhibit superior stability when they stand free on a rigid base (no isolation).

limit where the response of the heavy base is not influenced by the response of the light rocking block (decoupled system). Consequently for the case where $\gamma \leq 0.1$ the mass ration γ drops out of consideration (γ=0) and it can be eliminated from equations (33) and (34) – a conclusion that shows that the rocking response of a rigid block standing free on an isolated base exhibits a "complete similarity" in terms of the mass ratio $\gamma = \dfrac{m}{m+m_b}$.

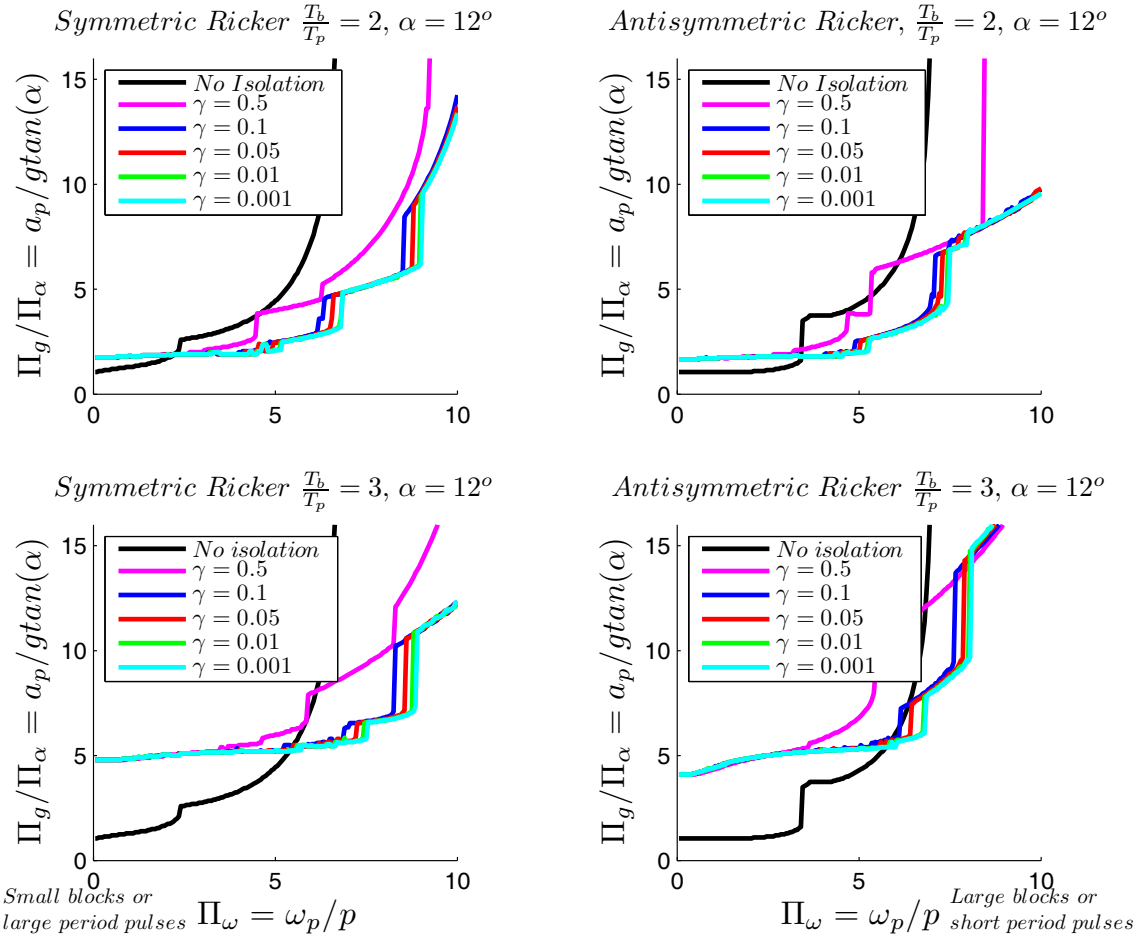

Figure 12 Comparison of the minimum acceleration needed to overturn a rigid block of slenderness α=12° resting on a linear viscoelastic isolated base subjected to a symmetric Ricker wavelet (left) and an antisymmetric Ricker wavelet (right). Results for five values of mass ratio $\gamma = \dfrac{m}{m+m_b}$ are used showing that for values of γ<0.1 the overturning acceleration does not depend on the mass ratio $\gamma = \dfrac{m}{m+m_b}$

6.3 Bilinear isolation system

When the behavior of the isolation system is bilinear – a very good idealization for the behavior of spherical sliding bearings and lead rubber bearings, the equation of the rocking block is again given by equation (19) whereas, horizontal equilibrium of the isolated base below isolators gives

$$-k_b u(t) - Q \cdot z(t) = m_b\left(\ddot{u}_g(t)+\ddot{u}(t)\right) + m\left(\ddot{u}_g(t)+\ddot{u}(t)+\ddot{x}(t)\right) \tag{45}$$

where k_b is the second slope of the bilinear idealization, Q is the strength of the system (force at zero displacement), $x(t)$ is the horizontal relative to the base translation of the center of mass of the rigid block and $z(t)$ is a dimensionless parameter of the Bouc-Wen model given by

$$\dot{z}(t) = \frac{1}{u_y}\left(\dot{u}(t) - \gamma\left|\dot{u}(t)\right| z(t)\left|z(t)\right|^{n-1} - \beta\dot{u}(t)\left|z(t)\right|^n\right), \tag{46}$$

where u_y is the yield displacement of the bilinear behavior.

In this paper our study concentrates in the case where u_y is very small ($u_y \approx 0.25$mm). In this case the bilinear model is the mathematical description of the spherical sliding bearing with coefficient of friction μ, in which case the strength $Q=\mu(m+m_b)g$. Recent studies (Makris and Chang [14], Makris and Vassiliou [30]), have demonstrated that the response of isolated structures is merely indifferent to the exact value of the yield displacement, therefore the results obtained in this paper are also valid for isolation systems that use lead rubber bearings (larger values of u_y) as long as they experience the same second slope and the same strength. Given equations (45) and (46), together with equation (19) the state vector of the system shown in Figure 2 (right) with spherical sliding bearings is:

$$\mathbf{y}(t)=\begin{bmatrix} u(t) \\ \dot{u}(t) \\ z(t) \\ \theta(t) \\ \dot{\theta}(t) \end{bmatrix} \tag{47}$$

$$\dot{\mathbf{y}}(t)=\begin{bmatrix} \dot{u}(t) \\ \dfrac{-\omega_b^2 u(t)-\mu g z(t)-\gamma R\left(\dot{\theta}(t)\right)^2 \sin A(t)+\gamma R\cos A(t)\, p^2 \sin A(t)}{1-\dfrac{\gamma R p^2 \cos^2 A(t)}{g}}-\ddot{u}_g(t) \\ \dfrac{1}{u_y}\left(\dot{u}(t)-\gamma\left|\dot{u}(t)\right|z(t)\left|z(t)\right|^{n-1}-\beta\dot{u}(t)\left|z(t)\right|^n\right) \\ \dot{\theta}(t) \\ -p^2\left(\sin A(t)+\cos A(t)\left(\dfrac{-\omega_b^2 u(t)-\mu g z(t)-\gamma R\left(\dot{\theta}(t)\right)^2 \sin A(t)+\gamma R\cos A(t)\, p^2 \sin A(t)}{g-\gamma R p^2 \cos A(t)}\right)\right) \end{bmatrix} \tag{48}$$

In the case where the base is isolated on lead rubber bearings exhibiting a strength Q, the term μg in the 1st and 5th component of the $\dot{\mathbf{y}}(t)$ vector is replaced with $\dfrac{Q}{m+m_b}$.

Figure 12 plots overturning spectra of a rigid block with slenderness $\alpha=16^o$ standing free on a base that is isolated on single concave spherical sliding bearings with coefficient of friction $\mu=5\%$ when subjected to a symmetric Ricker wavelet next to the overturning acceleration spectra when the base is isolated on linear viscoelastic bearings with coefficient $\xi=5\%$. The response between the two isolation configurations is very similar. For completeness, Figure 12 (bottom) shows the minimum overturning acceleration associated with the two isolation configurations together with the corresponding spectrum of a rigid block rocking on a rigid foundation (heavy dark line). The near-vertical growth of the heavy dark line indicates that regardless how flexible the isolation system is, for values of $\omega_p/p>6$, the rigid block rocking on a rigid foundation has superior stability. The seismic response of a rigid block standing free on a base that is isolated on double concave spherical sliding bearings is presented in the paper by Vassiliou and Makris [32].

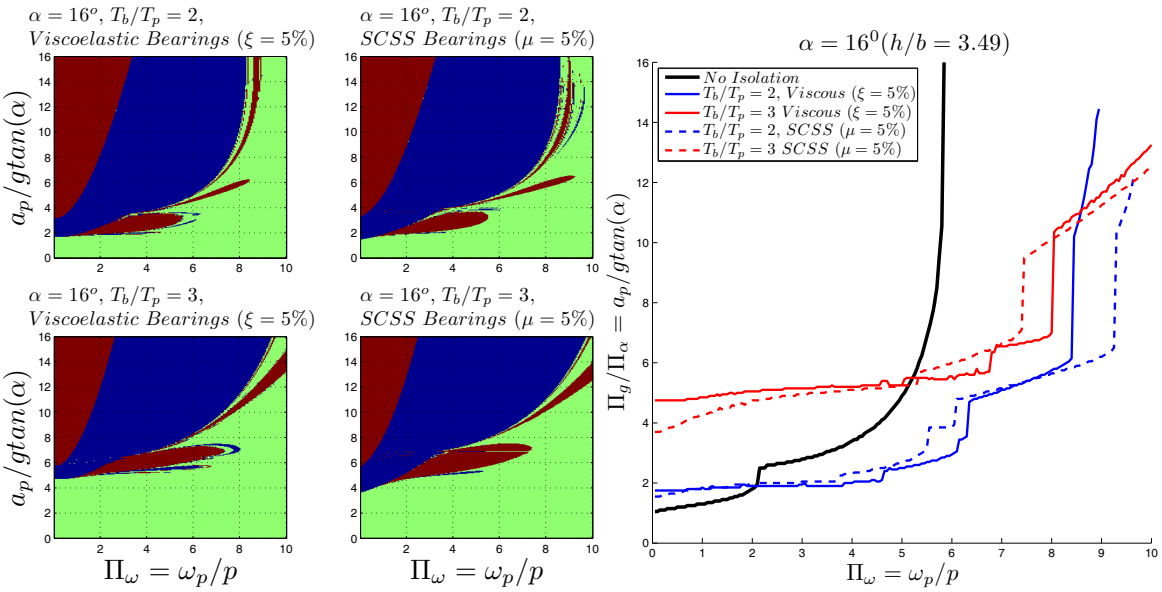

Figure 13. Comparison of overturning spectra (top) and minimum acceleration overturning spectra (bottom) of a rigid body with slenderness `a=16^o when the supporting base is isolated on viscoelastic bearings with damping ratio ξ=5% (left) and single concave spherical sliding bearings with coefficient of friction 5% (right). The excitation is a symmetric ricker wavelet and the mass ratio γ= 0.01

7 THE EFFECT OF SEISMIC ISOLATION ON ANCIENT CLASSICAL COLUMNS

The seismic response analysis of rocking blocks standing free on an isolated base has been studied in this paper by using as ground excitation, acceleration pulses described either by the symmetric or the antisymmetric Ricker wavelets. The acceleration amplitude, a_p, and duration T_p of any distinct acceleration pulse allow the use of the dimensional analysis presented in this work and the derivation of the associated Π-products which improve appreciably the understanding of the physics that governs the problem together with the organization and presentation of the response quantities in a most meaningful way. Nevertheless, in order to stress the main finding of this study – that for large blocks (say ω_p/p > 6) the use of seismic isolation reduces the seismic stability of free-standing rocking structures – we examine the seismic response of two free standing slender blocks which have the dimensions of the columns of the peristyle of the Temple of Appolo at Bassae and the Temple of Zeus at Nemea, both located in Peloponese, Greece.

The Temple of Apollo at Bassae is a fifth Century BC doric style structure. The columns of the temple are 5.95m high, the diameter of the base drum is 1.11m (resulting in slenderness α=0.1844 and in size R=3.03m). The number of drums in each column is not constant for all the columns and is controlled by the size of the sound rock that was available in the ancient limestone quarry. The temple is still standing but has suffered from erosion of the building material caused by the adverse climatic conditions at the site (1000m altitude a.s.l.) and from the tilting of some columns due to differential settlement of the foundations [32].

The Temple of Zeus at Nemea was built in the late fourth century BC. The columns of this temple are much taller and more slender than the ones of the temple at Bassae, reaching a height of 10.33 m. All columns consist of 13 drums and the base drum diameter is 1.52 m. The resulting slenderness is α=0.1461 and R=5.22m. This slenderness ratio is the smallest among the ancient Greek temples of continental Greece. Only one column of the peristyle and two columns of the pronaos of the Temple of Zeus remain standing from the ancient times.

While the columns from the two abovementioned Temples are multidrum, this investigation proceeds by considering that they are monolithic free standing blocks. Past studies led by the senior author (Konstantinidis and Makris, 2005 [33]) have shown that multidrum columns exhibit slightly more controlled response than the equal size monolithic configuration.

Our investigation proceeds by examining the response of the two abovementioned columns when subjected to the 11 historic records shown in Table 2. The columns are considered to stand free on a rigid foundation, or standing free on a seismic isolated base with isolation periods T_b=2s, 2.5s and 3s and linear viscous damping ξ_b=0.1.

Table 3 summarizes the results from the nonlinear time history analysis. The column from the Temple of Apollo at Bassae (R=3.03m α=0.1844) when standing free on a rigid foundation survives all the induced records, while when isolated on bearings that offer an isolation period, T_b=2.0s, it topples in all but one records. As the period of the isolation system increases the column survives additional records. Similarly, the column for the Temple of Zeus a Nemea (R=5.22m, α=0.1461) when standing free on a rigid foundation survives 9 out of the 11 records, while when isolated on bearings that offer an isolation period

Table 2. Earthquake records used for the dynamic response analysis of the column.

Earthquake	Record Station	Magnitude (Mw)	Distance (km)	PGA (g)	PGV (m/s)	a_p (g)	T_p (s)
1966 Parkfield	CO2/065	6.1	0.1	0.48	0.75	0.41	0.6
1977 Vrancea	Bucharest	7.2	160	0.20	0.74	0.20	2.1
1979 Imperial Valley	El Centro #6 / 230	6.5	9.3	0.41	0.65	0.14	3.1
1980 Irpinia, Italy	Sturno/270	6.5	32	0.36	0.52	0.11	3.0
1986 San Salvador	Geotech Investig. Center	5.4	4.3	0.48	0.48	0.34	0.8
1987 Superstition Hills	Parachute Test Site/225	6.7	0.7	0.45	1.12	0.30	2.0
1992 Erzican,	Erzincan/EW	6.9	13	0.50	0.64	0.34	0.9
1994 Northridge	Jensen Filter Plant/022	6.7	6.2	0.57	0.76	0.39	0.5
1995Kobe	Takarazuka/000	6.9	1.2	0.69	0.69	0.50	1.1
1999 Chi-Chi Taiwan	CHY101/E	7.6	11.2	0.35	0.71	0.10	3.5
1999 Chi-Chi Taiwan	CHY128/N	7.6	9.7	0.17	0.69	0.09	4.5

Table 3. Stability results for the rigid blocks corresponding to the columns of the Temples of Bassae and Nemea when subjected to the 11 earthquakes. (✓ = no overturn, × = overturn)

		Columns from the Temple of Apollo at Bassae (R=3.03m α=0.1844)				Columns from the Temple of Zeus at Nemea (R=5.22m, α=0.1461)			
Earthquake	Record Station	Non-Isolated	T_I=2s	T_I=2.5s	T_I=3s	Non-Isolated	T_I=2s	T_I=2.5s	T_I=3s
1966 Parkfield	CO2/065	✓	×	✓	✓	✓	×	×	✓
1977 Bucharest		✓	×	×	✓	✓	×	×	×
1979 Imperial Valley	El Centro #6 / 230	✓	×	×	×	✓	×	×	×
1980 Irpinia, Italy	Sturno/270	✓	×	×	×	✓	×	×	×
1986 San Salvador	Geotech Investig. Center	✓	×	✓	✓	✓	×	✓	✓
1987 Superstition Hills	Parachute Test Site/225	✓	×	×	×	×	×	×	×
1992 Erzican,	Erzincan/EW	✓	×	×	✓	×	×	×	×
1994 Northridge	Jensen Filter Plant/022	✓	×	×	×	✓	×	×	×
1995Kobe	Takarazuka/000	✓	×	✓	✓	✓	×	×	✓
1999 Chi-Chi Taiwan	CHY101/E	✓	✓	×	×	✓	×	×	×
1999 Chi-Chi Taiwan	CHY128/N	✓	×	✓	✓	✓	×	×	×

T_b=2.0s it topples in all records

Again, as the isolation period increases the column survives additional records; however, even when the isolation period is T_b=3.0s the column from the Temple of Zeus at Nemea survives only 3 out of the 11 records. The reason that seismic isolation is so detrimental to the stability of tall slender blocks is because the presence of the isolation system lengthens the duration of the pulses while at the same time increases the number of the significant induced cycles.

As an example, Figure 13 plots the response of a rigid block with the dimensions of a column of a column from the peristyle of the Temple of Zeus at Nemea subjected to the 022 component of the Jensen Filter Plant record from the 1994 Northridge earthquake when is standing free on a rigid foundation (left) and when standing free on an isolated base with T_b=3.0s (right).

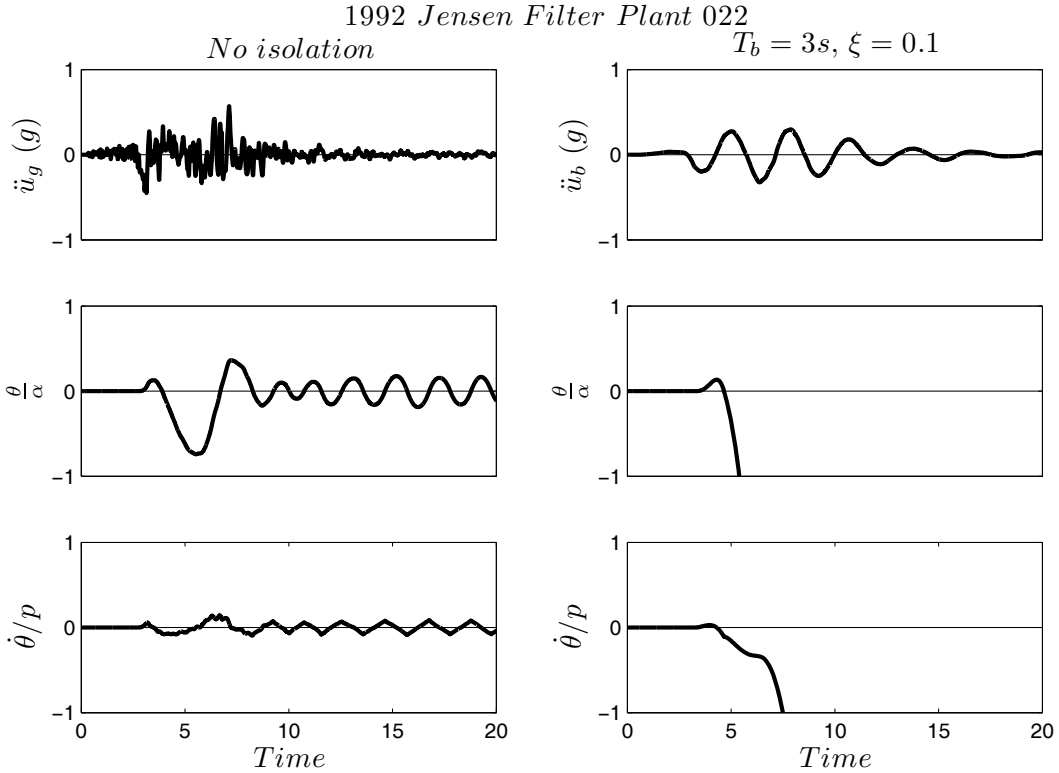

Figure 14. Comparison of the response of a rigid block with the dimensions of a column from the peristyle of the Temple of Zeus at Nemea subjected to the 022 component of the Jensen Filter Plant record from the 1994 Northridge earthquake when is standing free on a rigid foundation (left) and when standing free on an isolated base with T_b=3.0s (right).

8 CONCLUSIONS

In this paper the seismic response analysis and stability of slender rigid blocks standing free on a seismically isolated base is investigated in depth. The paper examines the rocking response when the isolated base is supported: (a) on linear viscoelastic bearings, (b) on single concave and (c) on double concave spherical sliding bearings. Our study revisits the equations of motion and settles the matter of conservation of linear momentum of the entire moving system that is the rocking – translating block together with the translating isolated base. This analysis leads to a closed form expression (eq. (32)) for the maximum value of the coefficient of restitution during impact that allows rocking motion of a block rocking on an isolated base and is concluded that this value is always smaller (more energy is dissipated) than the

maximum value, $r = \left(1 - \frac{3}{2}\sin^2\alpha\right)^2$ which is associated with a rigid block rocking on a rigid (non-isolated) foundation. Our extended parametric analysis concludes that seismic isolation is beneficial for small blocks. This happens because seismic isolation increases the "static" overturning acceleration; however for isolated rigid blocks this "static" value remains nearly constant as the ratio ω_p/p increases (moving to longer blocks or higher frequency pulses). Consequently, while the presence of an isolation base increases the "static" overturning acceleration it removes appreciably from the dynamics of rocking blocks the fundamental property of increasing stability as their size increases or the excitation pulse period decreases. This behavior prevails regardless whether the rocking block is supported on an isolated base with linear viscoelastic or spherical sliding bearings with single or double curvaruture.

The longer the isolation period of the supporting base is, the more stability is offered to the rocking blocks; however large blocks subjected to moderate period pulses (say $\omega_p/p>6$) exhibit superior stability when they stand free on a rigid base (non-isolated) rather when they are isolated even on isolation systems with very long periods. This remarkable result suggests that free standing ancient classical columns exhibit superior stability as they are built (standing free on a rigid foundation) rather than if they were seismic isolated. Consequently, seismic isolation is not recommended as a technology to improve the seismic stability of ancient Greek or Roman temples.

ACKNOWLEDGEMENTS

Partial financial support has been provided by the EU research project "DARE" ("Soil-Foundation-Structure Systems Beyond Conventional Seismic Failure Thresholds: Application to New or Existing Structures and Monuments"), which is funded through the 7th Framework Programme "Ideas", Support for Frontier Research – Advanced Grant, under contract number ERC-2—9-AdG 228254-DARE to Professor G. Gazetas.

Partial financial support has been provided to the second author by the Alexander S. Onassis Public Benefit Foundation.

REFERENCES

1.Housner, G. W. The behaviour of inverted pendulum structures during earthquakes. *Bulletin of the Seismological Society of America.* 1963; **53(2)**: 404–417.

2. G. Augusti, M. Ciampoli and L. Airoldi, 'Mitigation of seismic risk for museum contents', *Proceedings of the 10th world conference in earthquake engeineering*, Madrid 1992, pp.5995-6000

3. Vestroni F, Di Cinto S. Base isolation for seismic protection of statues. *Twelfth World Conference on Earthquake Engineering*, New Zealand, 2000.

4. Calio I, Marletta M. Passive control of the seismic response of art objects. *Engineering Structures* 2003; **25**: 1009–1018.

5. Roussis, PC, Pavlou, EA, Pisiara, EC. Base-isolation technology for earthquake protection of art objects, *14th World Conference on Earthquake Engineering: Innovation Practice Safety. 2008*

6. Contento A and Di Egidio A. Investigations into benefits of base isolation for non-symmetric rigid blocks, *Earthquake Engineering and Structural Dynamics* **38**(2009), pp. 849–866

7. Yim CS, Chopra AK, Penzien J. Rocking response of rigid blocks to earthquakes. *Earthquake Engineering and Structural Dynamics* 1980; **8**(6):565–587.

8. Makris N, Roussos Y. Rocking response of rigid blocks under near-source ground motions. *Geotechnique* 2000; **50**(3):243–262.
9. Zhang J, Makris N. Rocking response of free-standing blocks under cycloidal pulses. *Journal of Engineering Mechanics*, ASCE 2001; 127(5):473–483.
10. Veletsos AS, Newmark NM, Chelepati CV. Deformation spectra for elastic and elastoplastic systems subjected to ground shock and earthquake motions. *Proceedings of the 3rd World Conference on Earthquake Engineering*, vol. II, Wellington, New Zealand, 1965; 663–682.
11. Hall JF, Heaton TH, Halling MW, Wald DJ. Near-source ground motion and its effects on flexible buildings. *Earthquake Spectra* 1995; **11**(4):569 –605.
12. Heaton TH, Hall JF, Wald DJ, Halling MW. Response of high-rise and base-isolated buildings to a hypothetical Mw 7.0 blind thrust earthquake. *Science* 1995; **267**:206–211.
13. Makris N. Rigidity–plasticity–viscosity: can electrorheological dampers protect base-isolated structures from near-source ground motions? *Earthquake Engineering and Structural Dynamics* 1997; **26**:571–591.
14. Makris N, Chang S-P. Effect of viscous, viscoplastic and friction damping on the response of seismic isolated structures. *Earthquake Engineering and Structural Dynamics 2000*; **29**(1):85–107.
15. Alavi B, Krawinkler H. Effects of near-source ground motions on frame-structures. *Technical Report No. 138*, The John A. Blume Earthquake Engineering Center, Stanford University, 2001.
16. Mavroeidis GP, Papageorgiou AS. A mathematical representation of near-fault ground motions. *Bull. Seism. Soc. Am. 2003;* **93**(3):1099 –1131.
17. Aki K, Bouchon M, Chouet B, Das S. Quantitative prediction of strong motion for a potential earthquake fault. *Annali di Geofisica* 1977; 30:341–368.
18. Papageorgiou AS, Aki K. A specific barrier model for the quantitative description of inhomogeneous faulting and the prediction of strong ground motion. II. Applications of the model. *Bull. Seism. Soc. Am.* 1983; **73**:953–978.
19. Brune JN. Tectonic stress and the spectra of seismic shear waves from earthquakes. *Journal of Geophysical Research* 1970; **75**:4997–5009.
20. Aki K. Strong-motion seismology. In Earthquakes: Observation, Theory and Interpretation, Kanamori H, Boschi E (eds). *Proceedings of the International School of Physics, Enrico Fermi, Course 85*. North-Holland: Amsterdam, 1983; 223–250.
21. Makris N, Black CJ. Dimensional analysis of rigid-plastic and elastoplastic structures under pulse-type excitations. *Journal of Engineering Mechanics* (ASCE) 2004; **130**(9):1006–1018.
22. Makris N, Black CJ. Dimensional Analysis of Bilinear Oscillators under Pulse-Type Excitations *Journal of Engineering Mechanics* (ASCE) 2004 **130**(9) 1019-1031.
23. Karavasilis TL, Makris N, Bazeos N, Beskos DE Dimensional Response Analysis of Multistory Regular Steel MRF Subjected to Pulselike Earthquake Ground Motions, *J. Struct. Engrg.* 2010 **136**, 921-932 .
24. Ricker N. Further developments in the wavelet theory of seismogram structure. *Bulletin of the Seismological Society of America* 1943; **33,** 197-228.
25. Ricker N. Wavelet functions and their polynomials, *Geophysics* 1944 **9,** 314–323.
26. Addison P. *The Illustrated Wavelet Transform Handbook: Introductory Theory and Applications in Science, Engineering, Medicine and Finance*, Institute of Physics, London, UK, 2002.

27. Vassiliou MF, Makris N, Estimating time scales and length scales in earthquake acceleration records with the extended wavelet transform Report No. EEAM 2009-01, University of Patras, Greece, 2009.
28. Vassiliou MF, Makris N, Estimating time scales and length scales in pulselike earthquake acceleration records with wavelet analysis., *Bulletin of the Seismological Society of America.* 2011; **101(2)** DOI:10.1785/0120090387
29. MATLAB Version 2007b. *The Language of Technical Computing*. The Mathworks, Inc.: Natick, MA, 1999.
30. Makris N, Vassiliou MF. The existance of "complete similarities" in the response of seismic isolated structures subjected to pulse like ground motions and their implications in analysis. *Earthquake Engineering and Structural Dynamics* DOI:10.1002/eqe.1072
31. Psycharis IN, Papastamatiou DY, Alexandris AP. Parametric investigation of the stability of classical columns under harmonic and earthquake excitations. *Earthquake Engineering and Structural Dynamics* 2000; 29(8): 1093–1109.
32. Vassiliou MF, Makris N, Analysis of the rocking response of rigid blocks standing free on a seismically isolated base. *Earthquake Engineering and Structural Dynamics* (accepted for publication)
33. Konstantinidis D, Makris N. Seismic response analysis of multidrum classical columns. *Earthquake Engineering and Structural Dynamics* 2005; **34**(10):1243–1270.